An inverse analysis approach for the identification of the hygro-thermo-chemical model parameters of concrete

Massimiliano Bocciarelli[1]*, Gianluca Ranzi[2]

[1] Architecture, Built environment and Construction engineering Department, Politecnico di Milano (Technical University), Italy

[2] School of Civil Engineering, The University of Sydney, Australia

*Corresponding Author. E-mail: massimiliano.bocciarelli@polimi.it

Abstract

Hygro-thermo-chemical models provide useful representations of the mechanisms of moisture transport and temperature variations that take place in concrete structures and that can influence their durability and service behaviour. Several material parameters need to be specified when performing a hygro-thermo-chemical simulation. While some of these parameters can be evaluated based on the concrete mix specifications or from data reported in the literature, some other parameters are not readily available from the literature, partly because of their large variability and partly because they do not possess a precise physical meaning. In this context, this paper presents a robust inverse analysis procedure for the identification of this latter set of material parameters. The inverse analysis problem is formulated by using temperature and relative humidity profiles taking place within a concrete component as input. The proposed approach is applied to evaluate the minimum number of temperature and relative humidity measurements that are necessary to be performed for a successful identification of the sought material parameters. Representative results of an extensive sensitivity analysis are presented to gain insight into the most effective locations within the concrete component for the measurements and instants in time when these measurements should be collected. The inverse analysis procedure is then presented and validated against a set of pseudo-experimental results affected by different levels of noise, highlighting the robustness of the proposed methodology when applied with the arrangements suggested in terms of discrete relative humidity and temperature measurements and monitoring periods.

Keywords

Concrete; Hygro-thermo-chemical model; Identifiability; Inverse analysis; Model parameter characterisation

1. Introduction

Durability and serviceability limit states represent important requirements associated with the design of concrete structures. Excessive deformations, displacements and cracks may drastically affect the service behaviour of a structure and lead to increased maintenance costs. These effects are influenced by the time-dependent properties of the concrete and, in particular, by the physical and chemical mechanisms that take place in the concrete, especially in its early age. Moisture transport during hardening, occurring for release of water through the external surfaces and for internal water consumption due to chemical reactions such as cement hydration, causes volume changes that give rise to drying and autogenous shrinkage strains, respectively. The heat released during the cement hydration reaction may also cause volume changes inside the concrete. Different numerical and experimental studies on the early concrete behaviour exist in the literature and deal with the self-heating and self-drying phenomena. Bažant and Najjar [1] proposed a well-known material model for nonlinear moisture transport suitable for concrete and similar materials. This model was extended in subsequent years, for example, by including the direct modelling of the cement hydration occurring in concrete at early age by means of a thermodynamics based approach (e.g. [2]); by considering the aging effect on strength development through a coupled thermo-chemo-mechanical model (e.g. [3]) or, more recently, by taking into account the permeability increase once a macro crack is formed (e.g. [4]). Kim and Lee [5] and Oh and Cha [6] proposed a model for moisture and temperature calculation at concrete early age, where a sink term was added to the diffusive moisture equation to account for internal water consumption. A multi-phase coupled thermo-chemo-mechanical model was proposed by Gawin [7] and more recently by Du [8] and it accounted for the porous nature of the concrete by considering a micro-scale description of the material. The effects of the 3D meso-structure, modelled with different aggregate particles shapes and porous cement paste matrix, and of microcracks distribution on diffusivity and permeability of concrete materials has been studied in [9] and [10]. A new cement hydration model has been proposed in [11], considering the effects of C-S-H layers forming around anhydrous cement grains to control the very long hydration process which may occur in thick concrete components. Di Luzio et al. ([12] and [13]) proposed a hygro-thermo-chemical model by considering the effect of cement hydration on both moisture and temperature calculations in terms of internal water consumption and self-heating generation.

While the use of such hygro-thermo-chemical models provides great insight into the material behaviour, it requires the knowledge and input of several material parameters. The latter can be subdivided into two major sets: (i) one set of parameters that can be evaluated based on the concrete mix specifications or from data reported in the literature; and (ii) a second set of parameters that are characterised by a large variability (based on data available in the literature) and, among these, many parameters do not possess a precise physical meaning and, for this reason, are not amenable to a direct measurement. The inability of the latter set of parameters to be easily identified provides a limitation on the wider use of the hygro-thermo-chemical model.

In this context, this paper aims to provide a robust procedure for the identification of the set of material parameters for the hygro-thermo-chemical modelling defined at point (ii), i.e. parameters characterised by a large variability, some of which not amenable to a direct measurement because not reflecting a precise physical property. The proposed approach relies on the use of an inverse analysis procedure (see [14], [15] and [16]) that adopts temperature and relative humidity distributions as input data. The particularity of the proposed methodology is to give indication on the minimum number of temperature and relative humidity measurements that are required for a successful identification of the material parameters. This minimum requirement is established after evaluating through an extensive sensitivity analysis (of which representative results are presented in the following) the most effective locations and instants from concrete casting for the temperature and relative humidity measurements to take place through the thickness of a typical concrete component. The identification of the optimal locations and instants in time for the temperature and humidity measurements has significant practical implications, because supporting the effective planning of monitoring and measurement setups for laboratory or in-situ investigations. This becomes particularly significant considering the fact that recent technological advancements have led to a growing use and acceptance of temperature and relative humidity sensors embedded in concrete [17], for example, for its real-time strength monitoring. The outcomes of the proposed study will enable to optimise the number, locations and durations of the measurements while maximising the information collected.

In the first part of the paper, the hygro-thermo-chemical model is presented. In this section, a clear distinction is provided between the sets of parameters required by this model that can be determined from either the concrete mix specifications or from data available in the literature, and those that are characterised by a large variability and that are the focus of the present study. In view of using recorded temperature and relative humidity information as input in the inverse analysis process, the influence and responsiveness of the different material parameters on these two fields is discussed and representative trends are reported. The inverse analysis procedure is then introduced and its robustness is tested considering different scenarios constructed using pseudo-experimental data subjected to different degrees of noise. Representative results are provided to highlight the robustness of the proposed methodology when applied with the arrangements suggested for the discrete relative humidity and temperature measurements and with the recommended monitoring periods.

2. Hygro-thermo-chemical model

This section presents the hygro-thermo-chemical model capable to describe, over a spatial domain Ω, how the variations of the relative humidity h and temperature T take place over time t in a concrete component while accounting for different environmental conditions.

The model here adopted has been proposed in [12] and here applied, without any loss of generality, to a concrete mix without the presence of silica fume. The water transport mechanisms taking place in the concrete are described by the combination of the Fick's law, expressing the flux of water mass $\mathbf{j}$ as proportional to the gradient of the relative humidity h (i.e. $\mathbf{j} = -D_h \nabla h$) and the water mass balance equation, e.g. [1-12]:

$$\frac{\partial w}{\partial t} = \nabla \cdot \left[D_h \nabla h \right] \qquad \text{in } \Omega \tag{1}$$

where the total water content w depicts the sum of the evaporable water w_e and the non-evaporable water w_n, i.e. the water chemically bonded, for example, by cement hydration. The moisture diffusion D_h depends on the relative humidity h and temperature T as highlighted by the following expression [12]:

$$D_h(h,T) = \psi(T) D_1 \left[1 + \left(\frac{D_1}{D_0} - 1 \right) (1-h)^n \right]^{-1} \tag{2}$$

in which $\psi(T)$ (= $\mathrm{e}^{\left(E_{ad}/RT_0 - E_{ad}/RT\right)}$, with T_0 being the reference room temperature (taken as 296°K in the simulations presented in the following), considers the influence of the temperature on the moisture diffusion (see [18]), while it is usually assumed that $E_{ad}/R = 4700K$ (see e.g. [1]), and parameters D_0, D_1 and n depend on the specific concrete mix. In the literature, it is recognized that moisture diffusion depends on different transport mechanisms, which can be modelled individually to achieve a more physical description of the process. However, such an approach requires a series of information, such as concrete pore structure, pore radii and connectivity, that is usually not readily available or easily measurable from experimental tests. As this paper is focused at the identification of optimal or acceptable sets for practical experimental measurements, it is felt that the use of this single phenomenological law for the modelling of the different underlying physical mechanisms is acceptable, as also adopted by others in the literature [1,12].

Under the assumption that the non-evaporable water can be expressed as $w_n\left(\alpha_c\right) = k_c \alpha_c c$, with c being the cement ratio content and k_c a material parameter that, according to [12] and references herein, can be assumed equal to 0.253, and assuming the evaporable water to be expressed as a function of the relative humidity and of the degree of cement hydration α_c, i.e. $w_e = w_e\left(h, \alpha_c\right)$, Equation (1) can be rewritten as follows:

$$\frac{\partial w_e}{\partial h}\frac{\partial h}{\partial t} = \nabla \cdot \left[D_h \nabla h\right] - \left(\frac{\partial w_e}{\partial \alpha_c} + k_c c\right)\dot{\alpha}_c \qquad \text{in } \Omega \tag{3}$$

where the dot operator represents partial differentiation with respect to time t and α_c is calculated as the ratio between the level of hydration X_c and its theoretical asymptotic value $X_c^{\infty,th}$ exhibited in ideal hygro-thermal conditions. The maximum level of hydration at time infinity X_c^{∞} is usually assumed to remain below $X_c^{\infty,th}$ and, therefore, the maximum value of the reaction degree $\alpha_c^{\infty} = X_c^{\infty} / X_c^{\infty,th}$ is usually smaller than one, i.e. $\alpha_c^{\infty} < 1$. According to [19], we may assume $\alpha_c^{\infty} = \left(1.032\, w/c\right) / \left(0.194 + w/c\right)$, with *w/c* being the water-to-cement ratio.

Equation (3) highlights how the local variation of humidity depends on the divergence of the moisture flux and on two additional terms describing the microstructure variation (gel formation) and the internal consumption due to cement hydration.

The variation of α_c over time increases with relative humidity content and reduces while approaching its asymptotic value α_c^∞ as described by:

$$\dot{\alpha}_c = A_{c1}\left(\frac{A_{c2}}{\alpha_c^\infty}+\alpha_c\right)\cdot\left(\alpha_c^\infty-\alpha_c\right)\cdot e^{\left(-\frac{\eta_c\alpha_c}{\alpha_c^\infty}\right)}\cdot\frac{1}{\left[1+\left(a-ah\right)^b\right]}\cdot e^{\left(-\frac{\gamma_c}{T}\right)} \tag{4}$$

where $\gamma_c = E_{ac}/R$ with E_{ac} being the hydration activation energy and R the universal gas constant. Parameters A_{c1}, A_{c2} and η_c have no precise physical meaning and govern the so-called normalized chemical affinity. Constants a and b enter into the empirical function $b_h(h)=\left[1+\left(a-ah\right)^b\right]^{-1}$, which takes into account the slowing of the hydration process when relative humidity decreases below a certain value (around 80%). Their values are usually taken equal to a = 7.5 and b = 4.0 (see [1]).

The evaporable water can be expressed as a function of the relative humidity (sorption isotherm curve) as follows:

$$w_e\left(h,\alpha_c\right)=\kappa_{vg}^c\alpha_c c\left(1-1/\overline{e}_2\right)+\frac{w_0-0.188\alpha_c c-\kappa_{vg}^c\alpha_c c\left(1-1/\overline{e}_1\right)}{\left(\overline{e}_1-1\right)}\left(\overline{e}_2-1\right) \tag{5}$$

in which w_0 $\left(=\left(w/c\right)c\right)$ is the initial water content and it is assumed that $\overline{e}_2 = e^{10\left(g_1\alpha_c^\infty-\alpha_c\right)h}$ and $\overline{e}_1 = e^{10\left(g_1\alpha_c^\infty-\alpha_c\right)}$. Equation (5) depends on two other material parameters κ_{vg}^c and g_1 that govern the amount of water contained in the cement gel pores and the shape of the sorption curve, respectively. From equation (5), the moisture capacity $\partial w_e/\partial h$ is derived and inserted in equation (3).

The temperature field is calculated based on the Fourier's law, in which the heat flux **q** is expressed as a function of the temperature spatial gradient $\left(\mathbf{q} = \lambda \nabla T\right)$, and the enthalpy balance equation as follows:

$$\rho c_t \frac{\partial T}{\partial t} = \nabla \cdot \left[\lambda \nabla T\right] + \dot{Q}_c \qquad \text{in } \Omega \tag{6}$$

where T is the absolute temperature, λ is the heat conductivity that can be assumed constant for the temperature range considered in the present study, while ρ and c_t depict the concrete mass density and the specific heat, respectively, and $\dot{Q}_c$ represents the rate of heat generation due to cement hydration, calculated as $\dot{Q}_c = \dot{\alpha}_c c \tilde{Q}_c^{\infty}$, with $\tilde{Q}_c^{\infty}$ being the total heat content per unit cement mass due to cement hydration.

Equations (3) and (6) are coupled by their dependency on the degree of cement hydration α_c as well as by the moisture diffusion coefficient D_h that depends on both temperature and relative humidity.

The hygro-thermo-chemical model depends on a series of parameters. Some of them are well known concrete characteristics, whose values can be evaluated based on the concrete mix specifications or from data reported in the literature. These parameters are listed in the upper part of Table 1. Other parameters are characterised by a large variability (considering data available in the literature) and, among these, some do not possess a precise physical meaning. This set of parameters is listed in the lower part of Table 1 and their range of variation (obtained and derived from [12, 13, 20 and 21]) is collected in Table 2.

Table 1.

Table 2.

Table 3.

2.1 Finite element formulation

The hygro-thermo-chemical model described in Equations (3) and (6) is solved in the following by means of the finite element method, giving rise to the following discretized equations:

$$\begin{cases} \mathbf{W}\dot{\mathbf{H}} + \mathbf{D}\mathbf{H} = \mathbf{F} \\ \mathbf{C}\dot{\mathbf{T}} + \mathbf{\Lambda}\mathbf{T} = \mathbf{Q} \end{cases} \tag{7}$$

where **H** and **T** depict unknown vectors that collect all nodal values (of the finite element representation) of the relative humidity and temperature fields at each instant, while the system matrices are defined as:

$$\mathbf{W} = \bigcup_e \int_{\Omega_e} \mathbf{N}_e^T \frac{\partial w_e}{\partial h} \mathbf{N}_e \mathrm{d}\Omega \tag{8}$$

$$\mathbf{D} = \bigcup_e \int_{\Omega_e} \mathbf{B}_e^T D_h \mathbf{B}_e \mathrm{d}\Omega \tag{9}$$

$$\mathbf{F} = -\bigcup_e \int_{\Gamma_e} \mathbf{N}_e^T \mathbf{n}^T \mathbf{j} \,\mathrm{d}\Gamma - \bigcup_e \int_{\Omega_e} \mathbf{N}_e^T \left(\frac{\partial w_e}{\partial \alpha_c} + 0.253c \right) \dot{\alpha}_c \mathrm{d}\Omega \tag{10}$$

$$\mathbf{C} = \bigcup_e \int_{\Omega_e} \mathbf{N}_e^T \rho c_t \mathbf{N}_e \mathrm{d}\Omega \tag{11}$$

$$\mathbf{\Lambda} = \bigcup_e \int_{\Omega_e} \mathbf{B}_e^T \lambda \mathbf{B}_e \mathrm{d}\Omega \tag{12}$$

$$\mathbf{Q} = -\bigcup_e \int_{\Gamma_e} \mathbf{N}_e^T \mathbf{n}^T \mathbf{q} \,\mathrm{d}\Gamma + \bigcup_e \int_{\Omega_e} \mathbf{N}_e^T \dot{Q}_c \mathrm{d}\Omega \tag{13}$$

where symbol $\bigcup_e$ refers to the assembly operation typical of the finite element approach, and matrices $\mathbf{N}_e$ and $\mathbf{B}_e$ collect shape functions and their spatial derivatives, respectively.

For the solution of Equations (7), Dirichlet's boundary conditions (on *h* and *T*) are directly imposed on the unknown vectors **H** and **T**, while Cauchy's boundary conditions can be introduced in the right end side of the equation, see [22].

Equation (7) can be integrated over time by means of the so-called θ-method [22]:

$$\begin{cases} \left[\theta\mathbf{W}^{k+1}+(1-\theta)\mathbf{W}^{k}\right]\dfrac{\mathbf{H}^{k+1}-\mathbf{H}^{k}}{\Delta t}+ \\ \qquad \left[\theta\mathbf{D}^{k+1}+(1-\theta)\mathbf{D}^{k}\right]\left[\theta\mathbf{H}^{k+1}+(1-\theta)\mathbf{H}^{k}\right]=\left[\theta\mathbf{F}^{k+1}+(1-\theta)\mathbf{F}^{k}\right] \\ \left[\theta\mathbf{C}^{k+1}+(1-\theta)\mathbf{C}^{k}\right]\dfrac{\mathbf{T}^{k+1}-\mathbf{T}^{k}}{\Delta t}+ \\ \qquad \left[\theta\mathbf{\Lambda}^{k+1}+(1-\theta)\mathbf{\Lambda}^{k}\right]\left[\theta\mathbf{T}^{k+1}+(1-\theta)\mathbf{T}^{k}\right]=\left[\theta\mathbf{Q}^{k+1}+(1-\theta)\mathbf{Q}^{k}\right] \end{cases} \tag{14}$$

The above equations are approximated by taking the system matrices and the "load" vector at the previous instant *k* and by assuming $\theta = 1/2$ for the remaining term:

$$\begin{cases} \mathbf{W}^{k}\dfrac{\mathbf{H}^{k+1}-\mathbf{H}^{k}}{\Delta t}+\mathbf{D}^{k}\dfrac{\mathbf{H}^{k+1}+\mathbf{H}^{k}}{2}=\mathbf{F}^{k} \\ \mathbf{C}^{k}\dfrac{\mathbf{T}^{k+1}-\mathbf{T}^{k}}{\Delta t}+\mathbf{\Lambda}^{k}\dfrac{\mathbf{T}^{k+1}+\mathbf{T}^{k}}{2}=\mathbf{Q}^{k} \end{cases} \tag{15}$$

These equations are then solved with respect to the unknown vectors at instant *k+1*:

$$\begin{cases} \mathbf{H}^{k+1}=\left[\mathbf{W}^{k}+1/2\,\Delta t\mathbf{D}^{k}\right]^{-1}\left[\mathbf{W}^{k}\mathbf{H}^{k}+\Delta t\mathbf{F}^{k}-1/2\,\Delta t\mathbf{D}^{k}\mathbf{H}^{k}\right] \\ \mathbf{T}^{k+1}=\left[\mathbf{C}^{k}+1/2\,\Delta t\mathbf{\Lambda}^{k}\right]^{-1}\left[\mathbf{C}^{k}\mathbf{T}^{k}+\Delta t\mathbf{Q}^{k}-1/2\,\Delta t\mathbf{\Lambda}^{k}\mathbf{T}^{k}\right] \end{cases} \tag{16}$$

Time step Δt is not taken constant through the analysis but its value is increased as the simulation evolves since the rate of change of the mechanisms involved in the process decreases. In particular, after some convergence tests, Δt was taken equal to: 1200 s from the beginning to twice the curing time, then equal to 4 h up to 40 days, then 40 h up to 1 year and then equal to 400 h up to the final time. Optimized time steps strategies could have been investigated, in order to reduce the total computing time, but this was considered out of the scope of the present publication.

The use of the proposed numerical model is illustrated by evaluating the variations over time of the humidity profiles that occur in a typical concrete component exposed for drying and heat exchange through its top and bottom surfaces (Figure 1). With reference to the initial conditions adopted in the numerical analyses, at instant t=0 (instant of concrete casting and beginning of the curing period) relative humidity and temperature are set equal to 100% and 296 K (room temperature), respectively, and the degree of cement hydration is assumed null.

Two types of boundary conditions are considered in this study and these reflect possible conditions, such as those that could be specified in a laboratory environment when dealing with shrinkage measurements of concrete specimens, see figure 1:

- Curing phase. As for the humidity field, all sides are sealed by the formworks except for the upper side which is kept wet. For this reason on the lateral and lower sides of the finite element model zero-Cauchy boundary conditions are imposed while a relative humidity equal to 100% is assumed on the upper side of the model. These boundary conditions for the humidity field produce the loss of symmetry in figure 2. For the temperature field, it is assumed that the formworks are not able to impose perfect adiabatic conditions and, for this reason, the room temperature is assumed on both the upper and lower sides of the model. This selection of boundary conditions is preferred to test the proposed inverse algorithm with respect to the most unfavourable conditions because adiabatic conditions on the lower side would induce higher temperatures and, therefore, pseudo-experimental information more sensitive to the sought parameters. On the lateral sides of the finite element model adiabatic conditions are assumed.

- Drying phase. After the curing period, the lateral sides are sealed, for example, with plastic sheets to achieve relative humidity and heat fluxes along one direction only, i.e. along the thickness of the concrete component. For this reason, on the lateral boundaries of the finite element model zero-Cauchy boundary conditions are imposed, while on the upper and lower sides Dirichlet boundary conditions that enable heat and moisture exchange are imposed, as indicated in figure 1. These boundary conditions induce fluxes of heat and moisture across these boundaries due to the gradient of the relative field between the prescribed boundary value and that occurring inside the model.

The above boundary conditions induces quasi-1D solutions and, for this reason, the 2D model has been discretised by a structured mesh of three-nodes triangular elements, see figure 1, with 5 elements only through the width. The mesh has been refined close to the upper and lower boundaries where high spatial gradients are expected. After a convergence study and as a compromise between the conflicting requirement of accuracy and reduction of computing time, finite element discretizations with 300 elements and 213 nodes and 600 elements with 423 nodes, were adopted for the models 120 mm and 240 mm thick, respectively.

The results, in terms of humidity profiles, have been calculated for a period of 10 years and plotted in Figure 2 at different time increments. Two thicknesses have been considered for the concrete component, i.e. 120 mm (Figures 2a,b) and 240 mm (Figures 2c,d). Two external relative humidities (RHs) have adopted in the simulations and consist of 80% (Figures 2a,c) and 40% (Figures 2b,d). The material parameters used in the humidity predictions have been based on the mean values of ranges included in Table 2 and values specified in Table 3.

The results of Figure 2 highlight the ability of this model to simulate the highly non-linear humidity profiles that can develop through the thickness of a typical concrete component and how these can be influenced by the drying mechanism activated by the different external environmental conditions and due to the selection of different section heights and wet curing periods (results presented in Figure 2 have been calculated based on a wet curing period of 10 days). Figure 2a shows that, when exposed to a high relative humidity environment (i.e. environmental RH of 80%), a thin concrete component can approach an equilibrium condition of the entire cross-section with the ambient conditions after nearly a year from casting. This process is slower for a thicker concrete component as highlighted in Figure 2c with thickness of 240 mm in which, only after 10 years, equilibrium of the entire cross-section with the environment is achieved. When considering concrete components exposed to dry environments (with RH of 40%), steep humidity gradients occur in the 120 mm and 240 mm thick components and, even after 10 years, equilibrium of the entire cross-section is not obtained, as depicted in Figures 2b, d.

Figure 1.

Figure 2.

3. Sensitivity analysis

The design of the experiments, for inverse analysis purposes, can be improved by sensitivity analysis, which is intended to compute the influence of each sought parameter on the measurable quantities. The sensitivity analysis described in this section is used to gain a better understanding on how the sought material parameters, i.e. those listed in the lower part of Table 1, influence the variations of the relative humidity and temperature over time. In particular, the sensitivity analysis is applied to enhance the selection of the most effective time duration and spatial positions for the relative humidity and temperature measurements that will be considered and evaluated in the implementation of the inverse analysis technique in the following section, (see e.g., [23], [16]).

Sensitivity indices are computed as partial derivatives of relative humidity *h* and temperature *T* with respect to the model parameters p_i at a certain instant in time *t* (taking *t* = 0 the time of concrete casting) in a certain position *z* within the thickness of the concrete component as follows:

$$S_{h,p_i}\left(z,t,\boldsymbol{p}\right)=\frac{\partial h\left(\boldsymbol{p},z,t\right)}{\partial p_i}\frac{p_i}{h\left(\boldsymbol{p},z,t\right)} \tag{17a}$$

$$S_{T,p_i}\left(z,t,\boldsymbol{p}\right)=\frac{\partial T\left(\boldsymbol{p},z,t\right)}{\partial p_i}\frac{p_i}{T\left(\boldsymbol{p},z,t\right)} \tag{17b}$$

These indices are normalised, for comparison purposes, with respect to the parameter value and to the current and local value of the corresponding field. In the numerical computations, after some preliminary convergence studies, the (first-order) derivatives have been approximated by forward finite-differences with 0.1% increments, and have been evaluated in a number of locations through the thickness of the concrete component and for a certain number of time instants.

Figure 3 presents the sensitivity of the humidity profiles with respect to all model parameters through the thickness of the concrete component and at representative instants in time. These results have been obtained by assigning to the model parameters the mean values of Table 2 and those specified in Table 3, and by considering a 120 mm thick concrete component exposed on its top and bottom surfaces while applying a constant external temperature of 20°C and a relative humidity of 80%.

Figure 3.

The null sensitivity for all the parameters at the upper and lower sides of the model is due to the Dirichlet boundary conditions assumed. The curves plotted in Figure 3 highlight how the influence of the different model parameters on the relative humidity distributions varies in time and space. The time instants considered in the graphs of Figure 3 have been selected to outline both increasing and decreasing trends in the calculated sensitivity indices $S_{h,p_i}(z,t,\boldsymbol{p})$. In particular, it is possible to observe that there are two regions which present the highest sensitivities, with respect to all parameters, namely the mid-height of the concrete component and the position about 10 mm from the external surfaces. Among the plotted parameters governing moisture diffusion, the one which most affects the results in terms of humidity distribution is the exponent n, characterized by a sensitivity index ten times greater than the ones computed for parameters D_0 and D_1. It is interesting to observe that the sensitivity with respect to D_1, which represent the moisture diffusion at saturation ($h = 1$), reaches its peak value after 20 days and then it decreases with decreases in the humidity content. On the contrary, the sensitivity with respect to D_0, which represents the moisture diffusion at $h = 0$, keeps increasing for the first 180 days while the position of maximum sensitivity moves towards the mid-height of the concrete component as the desiccation process progresses. Sensitivity with respect to $Q_c^{\%0}$ is almost null since this parameter is expected to influence primarily the variation of the temperature field. Figure 4 depicts the sensitivity indices of the temperature profiles $S_{T,p_i}(z,t,\boldsymbol{p})$ computed only with respect to the parameters affecting this field, through the thickness of the concrete component and at selected time instants based on the concrete specimen and external environmental conditions described for $S_{h,p_i}(z,t,\boldsymbol{p})$.

Figure 4.

Figure 4 shows that the influence of the different model parameters on the temperature distribution is continuously varying in time and space. In particular, it is possible to observe that the region which presents the highest sensitivities, with respect to all parameters, is the mid-height of the concrete component. Another important conclusion which can be drawn from Figure 4 is that the highest sensitivity is achieved in the first few hours of the cement hydration chemical reaction, even if the time duration of the temperature variation phenomenon is about 2 days.

When considering the time variability of sensitivity indices for the humidity field (Figure 3), it is interesting to observe that the curves related to those parameters, which directly influence cement hydration (A_{c1}, A_{c2}, η_c and γ_c), present a first peak after the first 10-30 days and a second one (of opposite sign) after about 1 year. The time dependence associated with the sensitivity indexes is illustrated in Figure 5 for a concrete component 120 mm high and for a period of 10 years considering the highest $S_{h,p_i}\left(z,t,\boldsymbol{p}\right)$ (i.e. those determined for n, g_1, γ_c and η_c). For parameters governing moisture diffusion and sorption curves (n and g_1, respectively), the maximum value for $S_{h,p_i}\left(z,t,\boldsymbol{p}\right)$ is achieved between two and six months and after one month, respectively. The other two parameters (γ_c and η_c, governing cement hydration) present a maximum value after 30 days and a minimum after about one year.

Figure 5.

The trends depicted in Figure 5 for the 120 mm thick component exposed to an environmental RH of 80% are slightly modified when considering a dry environment (i.e. environmental RH = 40%) in Figure 6 and a larger thickness (i.e. 240 mm thick component) in Figures 7 and 8 with RH equal to 80% and 40%, respectively.

Figure 6.

Figure 7.

Figure 8.

In particular, Figure 6 (component with thickness of 120 mm and exposed to RH = 40%) shows how the peak values of the sensitivities are postponed in time. For example, the peak sensitivity for parameter n occurs after 4-5 years of casting (instead of 2-6 months observed with an ambient RH of 80%), and the peak and minimum values exhibited by g_1 along the different positions through the thickness take place after 1-2 months and 10-20 years, respectively (instead of the single peak observed after 1 month with RH = 80%). The variations for γ_c and η_c follow the trend exhibited by g_1, with the sensitivity peak soon after the pour (at about 1 month from casting) and the minimum after 2-3 years (instead of 12 months with ambient RH = 80%). These results highlight how the lower environmental relative humidity of 40% significantly extends the transient processes associated with the moisture movements due to the fact that it takes now longer time for the concrete component to find equilibrium through its entire height with the surrounding environment.

The sensitivity indices calculated for the thicker component (i.e. 240 mm) are presented in Figures 7a-d and 8a-d for ambient relative humidities of 80% and 40%, respectively. The overall differences observed for the two levels of external RH are similar to those noted for the 120 mm thick components in Figures 5 and 6, while the larger thickness leads to longer transfer processes to reach an equilibrium condition through the entire concrete component and, consequently, the instants in time of the peak and minimum points are postponed.

Based on the numerical tests carried out on the sensitivity analysis, the implementation of the inverse analysis approach presented in the following section will account for the fact that the positions characterized by the highest sensitivity are the mid-height of the component and close to its exposed surfaces for the humidity measurement, and just the mid-height for the temperature.

The highest sensitivity of the temperature field occurs in the first 6 hours from casting, when the humidity transport mechanism has almost not even started, as depicted by its negligible sensitivity. This means that measurements of the temperature distribution in this time interval are bound to enhance the identifiability of those parameters affecting this field, especially of those, cement hydration depends upon.

4. Inverse analysis

The inverse problem is usually defined as the minimization of a suitable norm, expressing the discrepancy between the experimental results and the numerical counterparts, computed as a function of the sought parameters.

The identifiability of the different parameters contained in the hygro-thermo-chemical model has been investigated following a numerical procedure well established in literature (see [24], [25] and [26]) that involves the setting up and implementation of different inverse analyses that start from the so-called pseudo-experimental results, i.e. results numerically generated starting from a given set of model parameters and supplied in input to the inverse problem. If this is well-posed, then its solution should provide in output the value of the parameters adopted to generate the pseudo-experimental data.

The input data for the inverse problem consists of both humidity and temperature profiles taken at different locations through the thickness of the concrete component and at different time instants. In particular, at each instant $\tau = 1 \ldots N_{ht}$ of the time history, relative humidity $h_{e,\tau s}$ is measured through the component thickness in a discretised number of locations, i.e. at

$s=1\ldots N_{hz}$. Similarly, at each instant $\tau=1\ldots N_{Tt}$, temperature $T_{e,\tau s}$ distribution is measured along the section in a discretised number of points $s=1\ldots N_{Tz}$. The discretization points adopted for both the space and time domains are based on the considerations obtained from the sensitivity analysis that highlighted the time instants and the spatial positions where the two fields are most affected by the sought parameters. Assuming to collect the model parameters to be estimated (i.e. those listed in the lower part of Table 1) in vector $\boldsymbol{p}$, and denoting experimental and computed quantities by subscript "e" and "c", respectively, the discrepancy between measured and computed quantities can be defined by the following norm:

$$w(\boldsymbol{p})=\phi_h\sum_{\tau}^{N_{ht}}\sum_{s}^{N_{hz}}\left[\frac{1}{h_{e,\tau s}^2}\left(h_{n,\tau s}(\boldsymbol{p})-h_{e,\tau s}\right)^2\right]+\phi_T\sum_{t}^{N_{Tt}}\sum_{s}^{N_{Tz}}\left[\frac{1}{T_{e,\tau s}^2}\left(T_{n,\tau s}(\boldsymbol{p})-T_{e,\tau s}\right)^2\right] \quad (18)$$

where $\phi_h=1/\left(N_{ht}N_{hz}\right)$ and $\phi_T=1/\left(N_{Tt}N_{Tz}\right)$ are weight factors whose magnitude ensure an equivalent contribution to be provided by the two terms defining the objective function.

The minimization of the function of Equation (19) is performed by the so-called Trust Region (TR) algorithm (see, e.g. [27] and [28]). Starting from a given initialization vector, this is automatically updated by means an iterative procedure based on subsequent evaluations of the objective function $w(\boldsymbol{p})$, of its gradients and on an approximation of the hessian matrix. The process stops when a priori tolerances on either the variation of the objective function or the Euclidean norm of the normalized optimization variables are met.

A deterministic batch approach is adopted in the present investigation, which means that uncertainties of both experimental measurements and system modelling are not processed stochastically, but the effect of random noise of different amplitude applied to the inverse problem input is considered in order to investigate the robustness of the proposed identification procedure. In particular, these disturbances are generated with uniform probability density over an interval centred on the exact amplitude.

For each adopted value of the parameters model $\boldsymbol{p}^{ad}$, the corresponding pseudo-experimental data are perturbated by different noise extractions $(n = 1 \ldots N_{NOISE})$. For each noise extraction, the optimization algorithm is run several times $(i = 1 \ldots N_{INIT})$ starting from different initialization vectors to avoid the solution to remain stuck in local minima that might exist given the nonlinear and non-convex nature of the objective function. The identified value, with respect to all initialization vectors, $\boldsymbol{p}_n^{id}$ is computed as average of all identified values $\boldsymbol{p}_{ni}^{id}$ weighted with respect to the inverse of the objective function in solution, as:

$$p_{n,k}^{id} = \frac{\sum_{i}^{N_{INIT}} p_{ni,k}^{id} \left(1 / w\left(\boldsymbol{p}_{ni}^{id} \right) \right)}{\sum_{i}^{N_{INIT}} \left(1 / w\left(\boldsymbol{p}_{ni}^{id} \right) \right)} \tag{19}$$

The error with respect to the assumed set of model parameters, for each noise extraction *n*, is then computed as:

$$err_{n,k}^{id} = 100 \cdot \left| \frac{p_{n,k}^{id} - p_k^{ad}}{p_k^{ad}} \right| \tag{20}$$

A final error index is then computed as the average of all the single errors computed for each noise extraction as follows:

$$err_k^{id} = \frac{1}{N_{NOISE}} \sum_{n}^{N_{NOISE}} err_{n,k}^{id} \tag{21}$$

This global error norm computes the average of the absolute values of the different errors resulting from the different noise extractions to avoid compensations between errors of opposite signs when a large number of random noise extractions is adopted.

4.1 Results

Different inverse analysis exercises have been solved in the following to investigate the optimal formulation of the inverse problem for the identification of the parameters characterised by a large variability (i.e. those listed in the lower part of Table 1), contained in the model presented in Section 2 on the basis of humidity and temperature profiles measurements. In the following, only representative results are presented to outline and support the key findings of this work.

The concrete properties adopted in the simulations are those equal to the means values of Table 2 and those specified in Table 3. Drying boundary conditions have been assumed on the two opposite surfaces of the concrete component (Figure 1) and the external temperature has been assumed constant and equal to 296 *K*.

The first inverse analysis exercise considers a 120 mm thick concrete component exposed to an environment relative humidity of 80%. In this initial simulation, no noise is added to the pseudo-experimental data. Figure 9 illustrates the convergence curves of the sought parameters (normalized with respect to the expected value) for two different initialization vectors.

Figure 9.

From these results, it is evident that the inverse problem is not well posed with respect to the identification of parameters A_{c1} and γ_c, identified with a weighted average error of 65.5% and 1.8%, respectively, while all the other parameters are identified with their expected value, with a maximum error of 0.2% for A_{c2}. The lack of identifiability of parameters A_{c1} and γ_c is related to the form in which they appear in the hygro-thermo-chemical model when defining $\dot{\alpha}_c$ in Equation (4). This is attributed to the fact that both parameters have an equivalent effect on $\dot{\alpha}_c$, i.e. an increase in A_{c1} leads to an increase of $\dot{\alpha}_c$ that could be similarly produced by a decrease of γ_c. Because of this behaviour, the inverse analysis procedure struggles to distinguish between these two parameters. This ill-posedness of the inverse problem is confirmed in Figure 10 that illustrates the variation of the objective function of Equation (18) plotted with respect to A_{c1} and γ_c.

Figure 10.

From this figure, it is evident the existence of different combinations of these two parameters providing the same absolute minimum of the objective function. However, due to its higher sensitivity, as highlighted, for example, in Figures 3 and 4 and also by the shape of the objective function in figure 10, γ_c can be still identified with a small error. The temperature T located in the denominator of the exponent of the exponential function of Equation (4) (with γ_c being located at the numerator of this exponent). provides only a marginal support to the identification of A_{c1} and γ_c, especially when considering realistic boundary conditions that enable heat exchange between the concrete component and its surrounding environment.

The above considerations have suggested that the following inverse analysis exercises will be carried out assuming A_{c1} known a priori. This assumption is considered valid based on the fact that the lack of identifiability of parameter A_{c1} previously discussed does not affect the identifiability of all other model parameters, see Figure 9. The validity of this assumption is later reconfirmed by the results reported in Table 6 outlining how different values for A_{c1} do not influence the identifiability of the sought parameters.

Representative results obtained from the inverse analysis procedure are presented in the following considering different arrangements for the discrete measurements of the relative humidity and temperature fields together with different periods of monitoring. Different concrete components and ambient conditions are used as case studies, for example varying their concrete thickness, period of wet curing after casting and ambient relative humidity. All pseudo-experimental results have been generated with a noise perturbation of ±10% to evaluate the robustness of the inverse procedure. It is considered that this noise is acceptable for the purpose of this study to take into account the inaccuracy and the disturbance associated with the experimental measurements.

Table 4 reports the results obtained considering a varying number of discrete humidity measurements through the thickness of the concrete component as well as the inclusion of a temperature measurement. The concrete component is 120 mm thick and wet cured for 1 day from casting. The ambient relative humidity is taken equal to 40% and the measurements are performed for a period of 30 days (with a frequency of one measurement per hour). Column A of Table 4 highlights how the use of one humidity measurement, even if selected at the mid-height of the concrete component that corresponds to the point of maximum sensitivity, is not sufficient for the sought parameters identification, the estimation of D_0 being affected by an error (21.7%) much larger than the added noise. The use of a second relative humidity measurement (located 10 mm below the exposed surface in column B of Table 4) ensures the identifiability of all parameters (the observed errors are within the magnitude of the noise introduced in the pseudo-experimental measurements). The inclusion of additional relative humidity measurements, for example at 20 mm and 30 mm below the exposed surface, does not improve the results as depicted by the values reported in columns C and D of Table 4.

The results outlined in columns E-G of Table 4 aim at evaluating the optimal position for the second humidity measurement for a 120 mm high concrete component and show that 10 mm below the exposed surface guarantees the identifiability of all parameters (column E), differently from the other choices implemented that struggle in the identification of D_0 (columns F and G). This result is consistent with the outcomes of the sensitivity analysis that shows a peak in this position (i.e. at 10 mm below the external surface) for the parameters governing moisture diffusion and sorption curves.

The results identified in columns A-G of Table 4 have been obtained considering one discrete temperature measurement located at its point of maximum sensitivity, i.e. mid-height of the concrete component, therefore highlighting the adequacy of using only the selected temperature measurement. The parameters identified without the inclusion of a temperature measurement (reported in column H of Table 4) do not lead to a successful characterisation of $\tilde{Q}_c^{\infty}$ and A_{c2}. These observations highlight how the use of a temperature measurement as experimental information is crucial for the identification of the model parameters $\tilde{Q}_c^{\infty}$ and A_{c2}, governing cement hydration, which cannot be identified if information on humidity distribution only are considered.

Table 4.

The influence of varying the period used for the monitoring of the relative humidity and temperature is presented in columns A-C of Table 5. For a concrete component with height of 120 mm, a period monitored of 30 days (column A) is sufficient for the identification of all model parameters. Longer periods of 60 days (column B) and 90 days (column C) seem not to improve the identifiability of the sought parameters.

The presence of a lower external relative humidity and, therefore, of a larger spatial gradient emphasizes the moisture transport phenomena and, consequently, improve the identifiability of all the parameters associated with this process. This is highlighted when comparing the results of columns A (RH 40%), with D and E (RH 80%) of Table 5, where it is shown that for a higher external humidity a longer monitoring period (90 days instead of 30 days) is needed to identify all the sought parameters.

Variations in the wet curing applied after concrete casting does not seem to influence the identifiability of the model parameters as, for example, depicted in columns A, F and G for wet curing periods of 1, 3 and 7 days, respectively. Curing periods approaching the monitored duration of the concrete component may jeopardize the identifiability of parameter D_0 governing moisture diffusion, as depicted in column H for a wet curing period of 14 days. Such a problem could be addressed by simply modifying the period monitored for the relative humidity measurements in order to gather sufficient experimental information after the end of the curing period (see column I).

Table 5.

At the beginning of this section, it has been shown that the parameters A_{c1} and γ_c could not be uniquely identified (Figures 9 and 10). The approach proposed in this paper to address this ill-posed condition has been to assign a value to A_{c1} equal to its mean value reported in the literature (=29450 s^{-1} based on the range provided in Table 2) before the application of the inverse analysis procedure. The results reported in Table 6 highlight how the identifiability of the model parameters is not affected when an incorrect value for A_{c1} (i.e. different from the one used for the generation of the pseudo-experimental measurements) is specified in input of the inverse analysis. In particular, the upper and lower limits of A_{c1} (see Table 2 for its range) are used in input for the results specified in columns B and C of Table 6 (with column A showing the errors determined using the exact value for A_{c1}, i.e. the value adopted to generate pseudo-experimental data). These results confirm that the identifiability of all parameters is not affected, except for the "companion" parameter γ_c, whose identification error increases, especially when the lower limit is assumed (however always within the same order of magnitude of the added noise for the cases considered).

Table 6.

The results discussed till now have been produced for a relatively thin concrete component with a thickness of 120 mm. Representative errors obtained in the case of a thicker component are outlined in Table 7. In this case, a longer period of measurements is needed and of at least 90 days (as depicted in Columns F and G) in order to let the moisture transport process develop sufficiently to collect the amount of experimental information needed for the calibration of the model parameters, especially of those governing moisture diffusion. Shorter monitored periods (reported in columns A-C for 30 days and in columns D and E for 60 days) do not provide sufficient experimental information. The use of two discrete measurements for the relative humidity is still required, with one measurement taken at the mid-height of the concrete component and the second one close to the exterior surfaces (errors reported in columns F and G consider the location of the second humidity measurement to be carried out at 10 mm and 30 mm, respectively, below the exterior surface).

Table 7.

5. Conclusions

This paper considers a hygro-thermo-chemical model capable of predicting temperature and moisture variations taking place over time in a concrete component and subdivides its parameters into two main sets: (i) one set of parameters that can be evaluated based on the concrete mix specifications or from data reported in the literature; and (ii) a second set of parameters that are characterised by a large variability and, in some cases, without a precise physical meaning and, therefore, not amenable to a direct measurement.

This paper presents a robust inverse analysis procedure for the identification of the second set of parameters using temperature and relative humidity measurements as input data. The aim of the present investigation is to provide an indication on the minimum (in time and space) number of discrete temperature and relative humidity measurements that are required for a successful identification of the sought material parameters. These results may find applications in enhancing the planning of the monitoring of in-situ investigations and of experimental tests.

Representative results have been presented to highlight the ability of the proposed methodology to identify correctly all the sought model parameters (within an error of the same order of magnitude of the noise added to the pseudo-experimental data in input to the inverse problem). The considerations listed below summarise the results observed for the specific case studies considered in this paper associated with the identification of the concrete parameters governing moisture and heat transport mechanisms:

- For the identification of the parameters governing the humidity field, at least two points within the height of the concrete component have to be monitored: one at the mid-height $\left(0.5\times D\right)$ and the second close to the exposed surface (preferably about 10 mm below the exterior surface for the 120 mm and 240 mm thick components considered in this study).
- The thicker the concrete component the larger the monitored period should be to let the moisture transport process develop sufficiently in order to gather the amount of experimental information needed to identify the model parameters. In the present analyses, for a concrete component 120 mm thick a period of 30 days (with a frequency of one measurement per hour) has been proven to be sufficient, while for a 240 mm thick component at least 90 days are required.
- Information on temperature field is crucial for the identification of the parameters governing the cement hydration. In the presented analyses, it has been shown that 1

measurement per hour taken at the mid-height of the concrete component (corresponding to the position with highest sensitivity) for a period of at least 48 hours from the time of casting is sufficient for the identification of the sought parameters.

- The presence of a lower external relative humidity emphasises the humidity transport mechanism and provides a better identification of the sought parameters, especially of those governing the moisture diffusion. If a larger humidity is applied (in the present examples 80% instead of 40%) the monitoring period should be increased (90 days instead of 30 days) in order to collect a sufficient amount of experimental information needed for the present identification purposes.

6. Acknowledgements

The work in this article was supported under the Australian Research Council's Discovery Projects funding scheme (project number DP140400529).

References

[1] Bažant ZP, Najjar LJ. Nonlinear water diffusion in nonsaturated concrete. Materiaux et Constructions 1972;5:3–20.

[2] Ulm FJ, Coussy O. Modeling of thermo-chemical–mechanical couplings of concrete at early age. Journal of Engineering Mechanics ASCE 1995;121:785–94.

[3] Cervera M, Oliver J, Prato T. Thermo–chemo–mechanical model for concrete. I: hydration and aging. Journal of Engineering Mechanics ASCE 1999;125:1018–1027.

[4] Gasch T, Malm R, Ansell A. A coupled hygro-thermo-mechanical model for concrete subjected to variable environmental conditions. International Journal of Solids and Structures 2016;91:143–156.

[5] Kim JK, Lee CS. Moisture diffusion of concrete considering self-desiccation at early ages. Cement and Concrete Research 1999;29:1921–1927.

[6] Oh BH, Cha SW. Nonlinear analysis of temperature and moisture distributions in early-age concrete structures based on degree of hydration. ACI Materials Journal 2003;100:361–70.

[7] Gawin D, Pesavento F, Schrefler BA. Hygro-thermo-chemo-mechanical modelling of concrete at early ages and beyond, Part I: hydration and hygrothermal phenomena. International Journal Numerical Methods Engineering 2006;67:299–331.

[8] Du M, Jin X, Ye H, Jin N, Tian Y. A coupled hygro-thermal model of early-age concrete based on micro-pore structure evolution. Construction and Building Materials 2016;111:689–698.

[9] Abyaneh SD, Wong HS, Buenfeld NR. Modelling the diffusivity of mortar and concrete using a three-dimensional mesostructure with several aggregate shapes. Computational Materials Science 2013;78:63–73.

[10] Abyaneh SD, Wong HS, Buenfeld NR. Simulating the effect of microcracks on the diffusivity and permeability of concrete using a three-dimensional model. Computational Materials Science 2016;119:130–143.

[11] Rahimi-Aghdama S, Bažant ZP, Abdolhosseini Qomic MJ. Cement hydration from hours to centuries controlled by diffusion through barrier shells of C-S-H. Journal of the Mechanics and Physics of Solids 2017;99:211–224.

[12] Di Luzio G, Cusatis G. Hygro-thermo-chemical modeling of high performance concrete. I: Theory. Cement & Concrete Composites 2009;31:301–308.

[13] Di Luzio G, Cusatis G. Hygro-thermo-chemical modeling of high performance concrete. II: Numerical implementation, calibration, and validation. Cement & Concrete Composites 2009;31:309–324.

[14] Bui HD. Inverse Problems in the Mechanics of Materials: an Introduction. CRC Press, Boca Raton FL, 1994.

[15] Mroz Z, Stavroulakis GE. Identification of Materials and Structures. CISM Lecture Notes, Vol. 469, Springer-Verlag, Wien, 2005.

[16] Stavroulakis G, Bolzon G, Waszczyszyn Z, Ziemianski L. Inverse analysis, in: B Karihaloo, RO Ritchie, I Milne (Eds.). Comprehensive Structural Integrity, Elsevier Science Ltd., Kidlington (Oxfordshire), UK, 2003.

[17] Digital Humidity Sensor SHT7x (RH/T). https://www.sensirion.com/products/humidity-sensors/pintype-digital-humidity-sensors/, 2017 [accessed 05.05.17].

[18] Jooss M. Reinhardt HW, Permeability and diffusivity of concrete as function of temperature. Cement Concrete Research 2002;32:1497–1504.

[19] Pantazopoulo SJ, Mills RH. Microstructural aspects of the mechanical response of plain concrete. ACI Materials Journal 1995;92:605–616.

[20] Di Luzio G, Cusatis G. Solidification–microprestress–microplane (SMM) theory for concrete at early age: Theory, validation and application. International Journal of Solids and Structures 2013;50:957–975.

[21] Wan L, Wendner R, Liang B, Cusatis G. Analysis of the behavior of ultra high performance concrete at early age. Cement and Concrete Composites 2016;74:120–135.

[22] Quarteroni A. Modellistica numerica per problemi differenziali. Springer-Verlag Italia, Milano, 2000.

[23] Kleiber M, Antúnez H, Hien TD, Kowalczyk P. Parameter Sensitivity in Nonlinear Mechanics, Theory and Finite Element Computations. John Wiley & Sons, Chichester, 1997.

[24]. Bocciarelli M, Buljak V, Moy CKS, Ringer SP, Ranzi G. An inverse analysis approach based on a POD direct model for the mechanical characterization of metallic materials. Computational Materials Science 2014;95:302–308.

[25] Bolzon G, Talassi M. An effective inverse analysis tool for parameter identification of anisotropic material models. International Journal of Mechanical Sciences 2013;77:130–144.

[26] Ardito R, Cocchetti G. Statistical approach to damage diagnosis of concrete dams by radar monitoring: Formulation and a pseudo-experimental test. Engineering Structures 2006;28:2036–2045.

[27] Coleman TF, Li Y. SIAM Journal of Optimization 1996;6:418–445.

[28] The Math Works Inc, USA, User's Guide and Optimization Toolbox, Release 6.13, Matlab 2004.

Table 1. Material parameters required in input of the hygro-thermo-chemical model.

	Parameter	Description
Parameters calculated based on concrete mix specifications or assigned known values well accepted in the literature	c	cement content
	w/c	water-to-cement ratio
	a, b	parameters associated with the variation of the degree of cement hydration over time and taken as a = 7.5 and b = 4.0 [1]
	λ	heat conductivity
	ρ	concrete mass density
	c_t	concrete specific heat
	k_c	parameter associated with non-evaporable water and taken as 0.253 (as suggested in [12])
Parameters characterised by a large variability (see Table 2) – some of which do not possess a precise physical meaning (to be identified with the inverse analysis presented in Section 4)	A_{c1}, A_{c2}, η_c	parameters with no precise physical meaning associated with the variation of the degree of cement hydration over time
	γ_c	parameter calculated as the ratio of the hydration activation energy over the universal gas constant
	$\tilde{Q}_c^{\infty}$	total heat content per unit cement mass due to cement hydration
	κ_{vg}^{c}	parameter that governs the amount of water contained in the cement gel pores
	g_1	parameter that governs the shape of the sorption curve
	D_0, D_1, n	parameters that control the moisture permeability and depend on the specific concrete mix

Table 2. Range of variation for the parameters listed in the lower part of Table 1.

Parameter	Range of variation	Mean value
A_{c1}	3900 – 55000 [s^{-1}]	29450
A_{c2}	10^{-6} – $5\cdot10^{-2}$	$2.5\cdot10^{-2}$
η_c	5.5 – 8.0	6.75
γ_c	3000 – 8000 [K]	5500
$\tilde{Q}_c$	400 – 550 [kJ/kg]	475000
κ_{vg}^{c}	0.10 – 0.26	0.18
g_1	1.20 – 2.20	1.70
D_0/c	$0.2\cdot10^{-14}$ – $7.5\cdot10^{-14}$ [m^2/s]	$3.85\cdot10^{-14}$
D_1/c	$4.8\cdot10^{-10}$ – $12\cdot10^{-10}$ [m^2/s]	$8.4\cdot10^{-10}$
n	3.0 – 4.5	3.75

Table 3. Parameters used in the proposed numerical simulations.

Parameter	Assumed value
c	400 kg/m^3
w/c	0.40
a	5.5
b	4.0
λ	2.3 W/mºC
ρ	2400 kg/m^3
c_t	1100 J/kgºC
k_c	0.253

Table 4. Results of the inverse analysis exercises in terms of err_k^{id} [%]: varying location of discrete measurements for the relative humidity *h* and the temperature *T*.

D [mm]	120							
RH	40%							
Period of wet curing	1 day							
Period monitored	30 days							
Location of discrete measurements[1]								
for *h* [mm]	60	60/10	60/20/10	60/30/20/10	60/10	60/20	60/30	60/10
for *T* [mm]	60				60			none
Column	A	B	C	D	E	F	G	H
D_0	21.7	5.9	4.5	5.2	5.9	11.9	14.7	6.3
D_1	3.1	3.9	2.9	4.8	3.9	2.9	3.1	7.2
n	3.3	0.7	0.6	1.0	0.7	1.7	2.5	0.8
κ_{vg}^{c}	7.1	2.5	2.0	2.2	2.5	3.1	7.3	7.2
g_1	5.4	3.7	3.6	4.7	3.7	5.3	4.1	6.6
γ_c	0.1	0.3	0.2	0.2	0.3	0.2	0.1	1.5
$\tilde{Q}_c^{\infty}$	4.4	2.4	1.8	3.5	2.4	4.2	2.2	11.1
A_{c2}	6.5	5.6	5.4	4.7	5.6	6.3	5.9	37.8
η_c	6.2	3.1	3.2	4.4	3.1	5.1	4.5	5.5

NOTE: [1]Locations measured from external surfaces of concrete component [mm].

Table 5. Results of the inverse analysis exercises in terms of err_k^{id} [%]: varying the period monitored, the external relative humidity RH and the period of wet curing after casting.

D [mm]	120								
Location of discrete measurements for *h* [mm][1]	60/10								
Location of discrete measurements for *T* [mm][1]	60								
Period monitored [days]	30	60	90	30	90	30			14+29[2]
RH	40%			80%	80%	40%			40%
Period of wet curing [days]	1			1	1	3	7	14	14
Column	A	B	C	D	E	F	G	H	I
D_0	5.9	3.3	4.4	10.3	8.7	7.1	7.9	13.3	5.0
D_1	3.9	3.0	2.4	3.6	3.3	2.8	2.5	2.5	3.9
n	0.7	0.5	0.6	1.2	0.8	1.0	1.2	2.0	0.7
κ_{vg}^{c}	2.5	1.9	2.4	4.0	5.0	2.4	2.6	2.8	1.7
g_1	3.7	4.1	2.5	4.9	4.3	2.6	3.7	2.4	5.0
γ_c	0.3	0.2	0.2	0.1	0.1	0.1	0.1	0.1	0.1
Q_c^{∞}	2.4	2.8	1.6	3.0	2.0	2.7	3.1	1.7	3.8
A_{c2}	5.6	5.4	4.0	3.2	4.4	4.4	5.2	5.1	4.1
η_c	3.1	3.5	1.8	3.7	2.7	2.4	4.4	2.8	5.2

NOTE: [1]Locations measured from external surfaces of concrete component [mm].
[2]Period monitored for the relative humidity measurements after the completion of the wet curing period.

Table 6. Results of the inverse analysis exercises in terms of err_k^{id} [%]: varying the period monitored, the external relative humidity RH and the period of wet curing after casting.

D [mm]	120		
RH	40%		
Period of wet curing	1 day		
Period monitored	30 days		
Location of discrete measurements for *h* [mm][1]	60/10		
Location of discrete measurements for *T* [mm][1]	60		
Parameter A_{c1} [s^{-1}]	29450	3900	55000
Column	A	B	C
D_0	5.9	6.0	6.4
D_1	3.9	4.5	4.1
n	0.7	0.7	0.7
κ_{vg}^{c}	2.5	3.2	2.6
g_1	3.7	4.7	3.7
γ_c	0.3	10.8	2.9
$\tilde{Q}_c^{\infty}$	2.4	2.8	2.3
A_{c2}	5.6	5.2	5.0
η_c	3.1	3.4	2.7

NOTE: [1]Locations measured from external surfaces of concrete component [mm].

Table 7. Results of the inverse analysis exercises in terms of err_k^{id} [%]: varying the period monitored and the location of the discrete measurements for the relative humidity for a thicker concrete component.

D [mm]	240						
RH	40%						
Period of wet curing	1 day						
Location of discrete measurements for *T* [mm][1]	120						
Period monitored [days]	30			60		90	
Location of discrete measurements for *h* [mm][1]	120/10	120/20	120/30	120/10	120/30	120/10	120/30
Column	A	B	C	D	E	F	G
D_0	7.8	16.2	27.9	5.0	7.0	3.3	6.1
D_1	6.7	5.1	4.9	5.7	5.4	3.4	3.2
n	1.1	3.1	3.2	0.8	1.0	0.6	0.9
κ_{vg}^{c}	5.1	6.6	9.7	5.6	10.6	5.7	5.8
g_1	6.7	8.5	8.8	5.1	8.1	4.1	3.7
γ_c	0.5	0.4	0.3	0.4	0.5	0.2	0.2
Q_c^{∞}	2.8	4.9	3.4	1.5	2.1	1.5	1.1
A_{c2}	13.4	10.1	10.1	11.5	14.1	6.4	6.4
η_c	5.7	7.6	6.2	4.0	5.4	2.3	2.3

NOTE: [1]Locations measured from external surfaces of concrete component [mm].

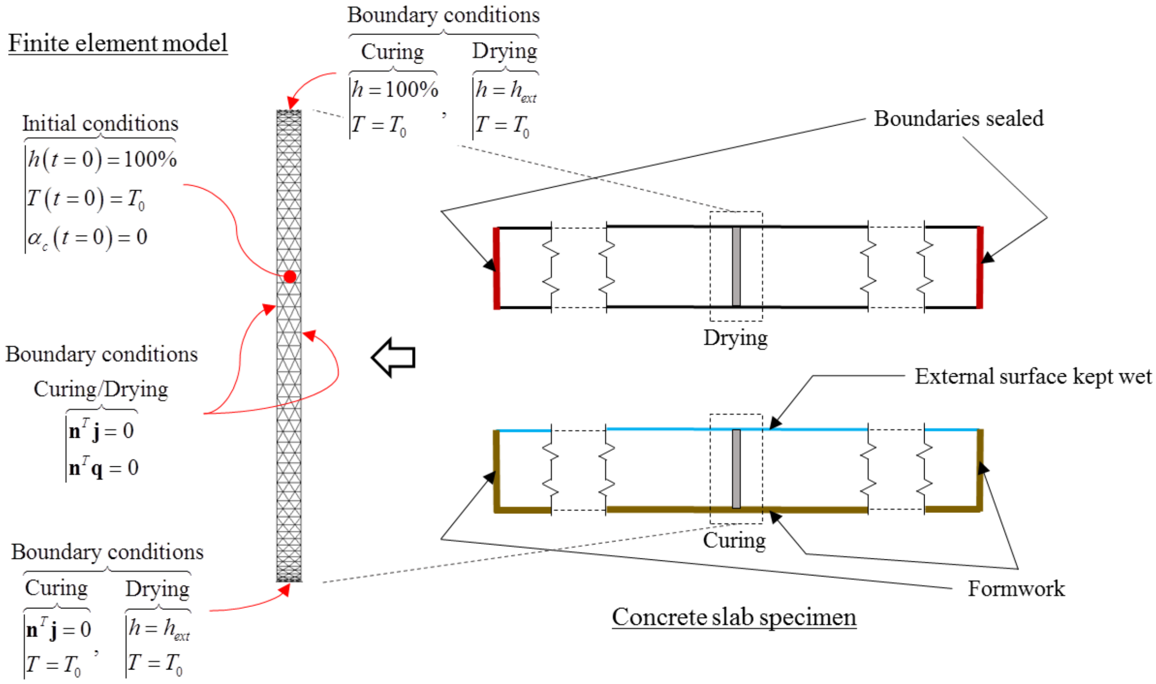

Figure 1. Typical concrete component used in the simulations: finite element model, initial and boundary conditions.

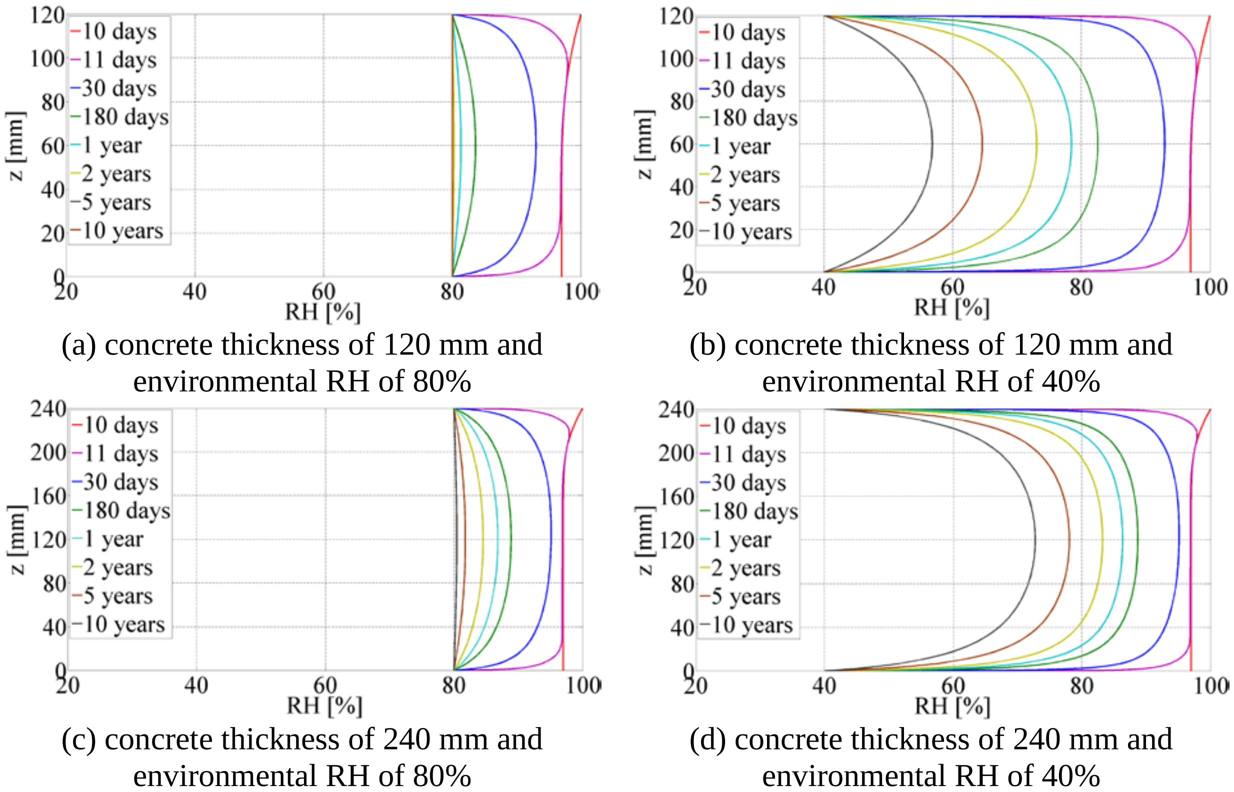

(a) concrete thickness of 120 mm and environmental RH of 80%

(b) concrete thickness of 120 mm and environmental RH of 40%

(c) concrete thickness of 240 mm and environmental RH of 80%

(d) concrete thickness of 240 mm and environmental RH of 40%

Figure 2. Humidity profiles for 10 years of simulation

for typical concrete components (Figure 1) with thicknesses of 120 mm and 240 mm.

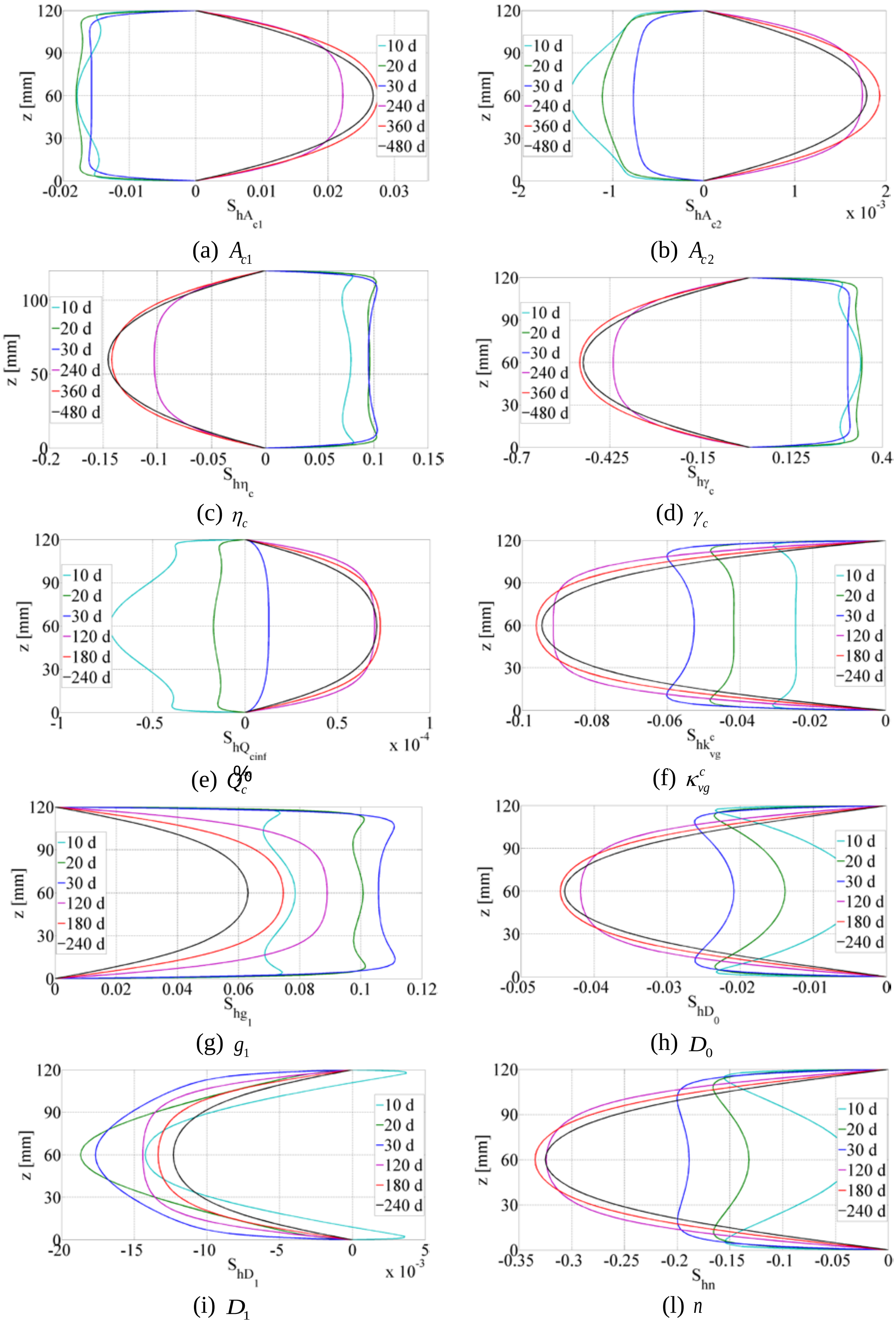

Figure 3. Sensitivity of humidity profiles with respect to the different model parameters.

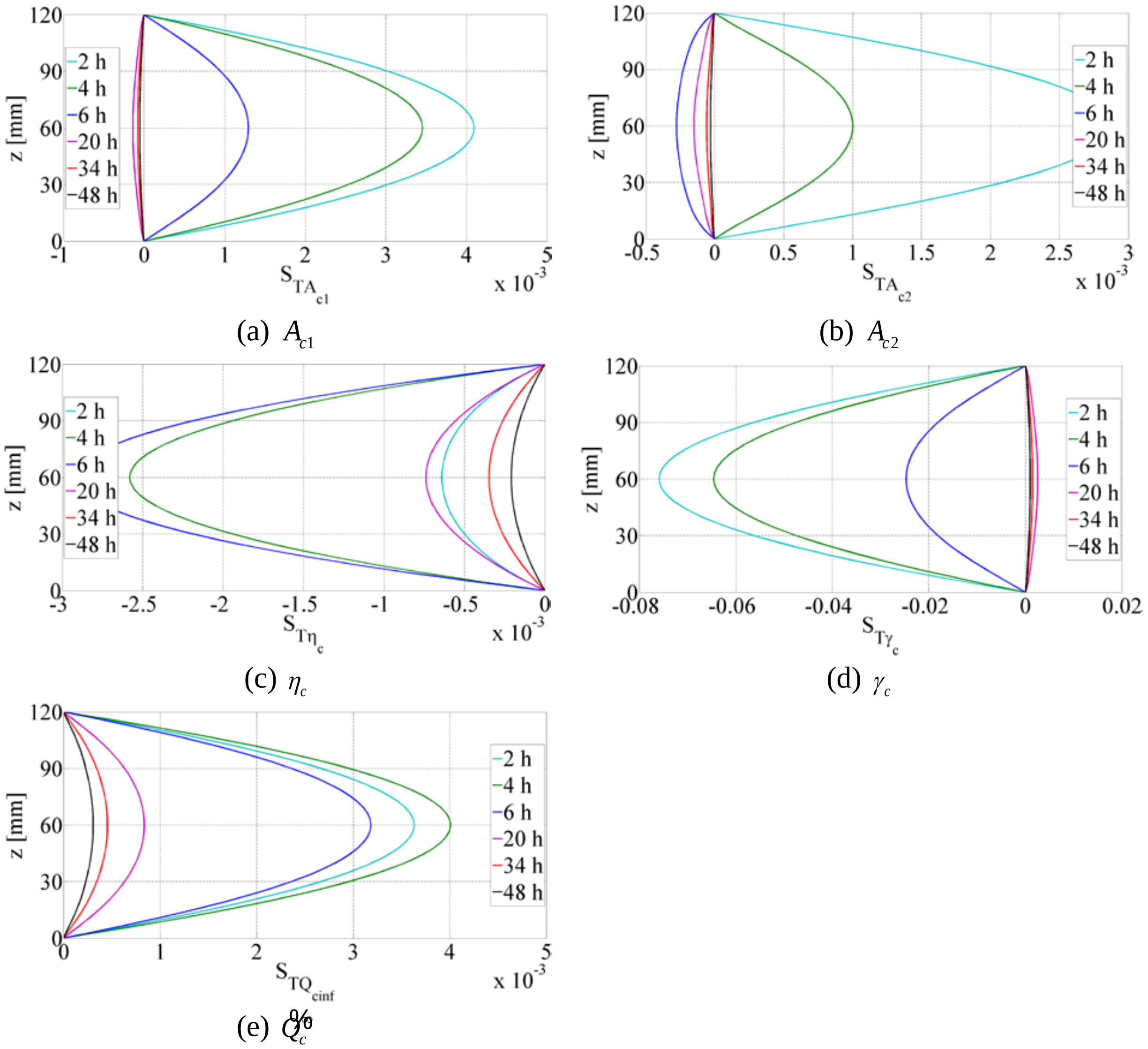

Figure 4. Sensitivity of temperature profiles with respect to the selected model parameters.

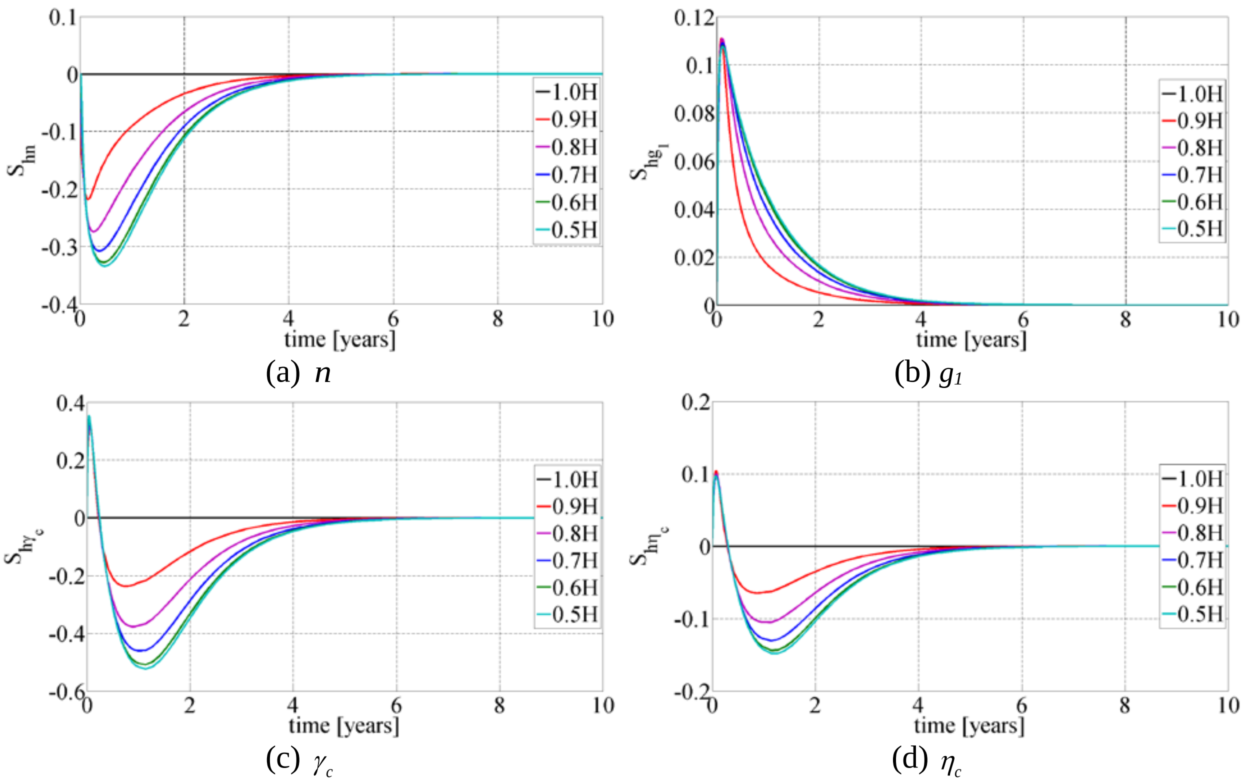

Figure 5. Time dependence of the maximum sensitivity indices at selected locations through the concrete component height H of 120 mm exposed to an ambient RH of 80%.

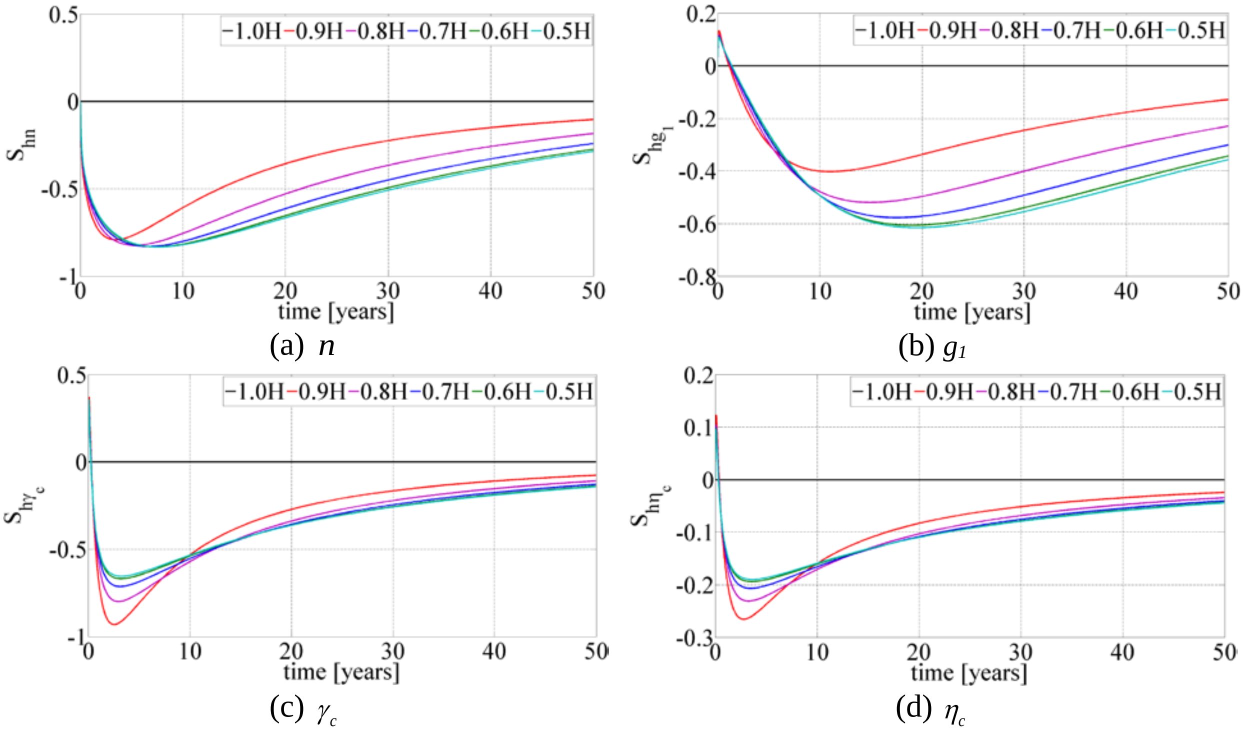

Figure 6. Time dependence of the maximum sensitivity indices at selected locations through the concrete component height H of 120 mm exposed to an ambient RH of 40%.

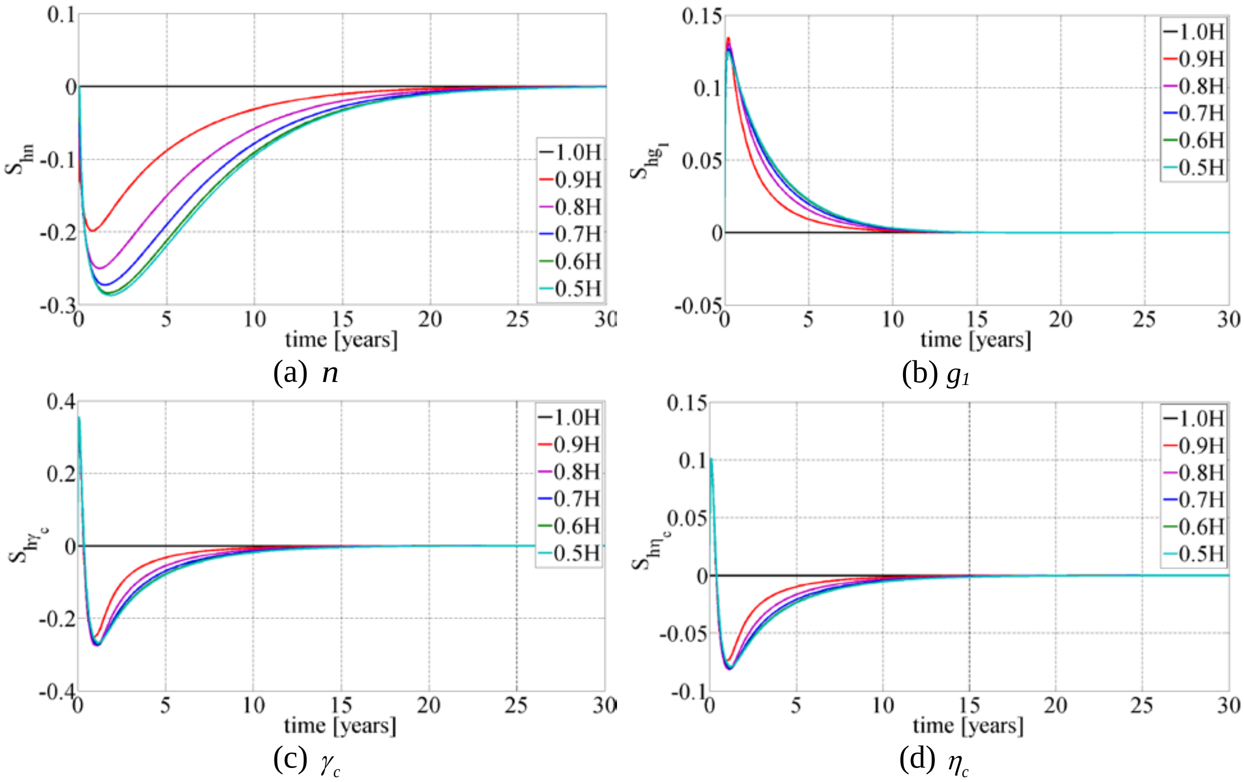

Figure 7. Time dependence of the maximum sensitivity indices at selected locations through the concrete component height H of 240 mm exposed to an ambient RH of 80%.

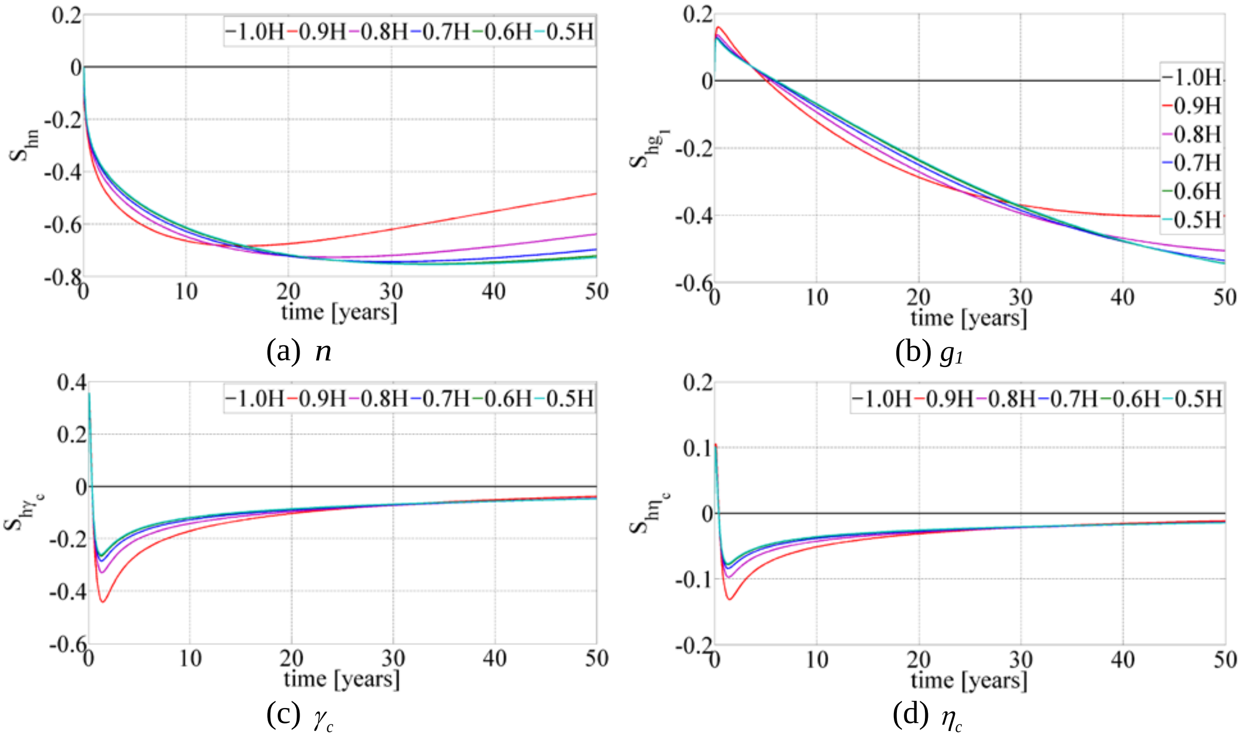

Figure 8. Time dependence of the maximum sensitivity indices at selected locations through the thickness of the 240 mm concrete component exposed to an ambient RH of 40%.

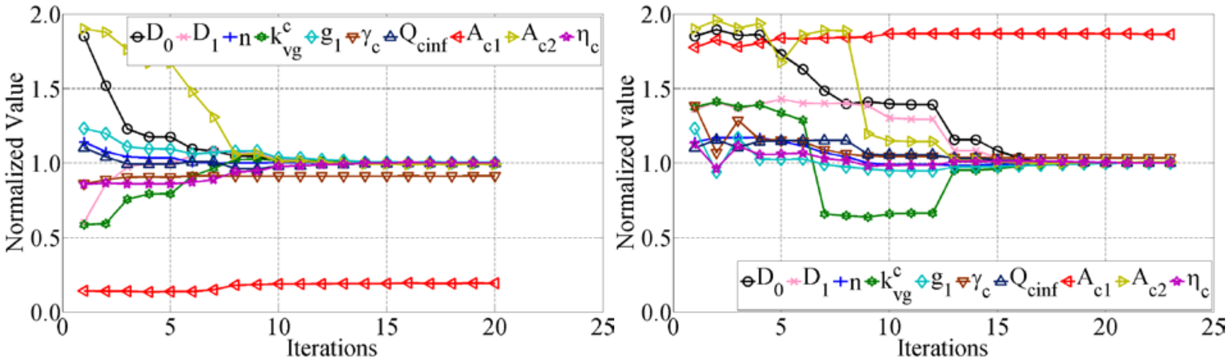

Figure 9. Convergence curves of the sought parameters (normalized with respect to the expected value) for two different initialization vectors.

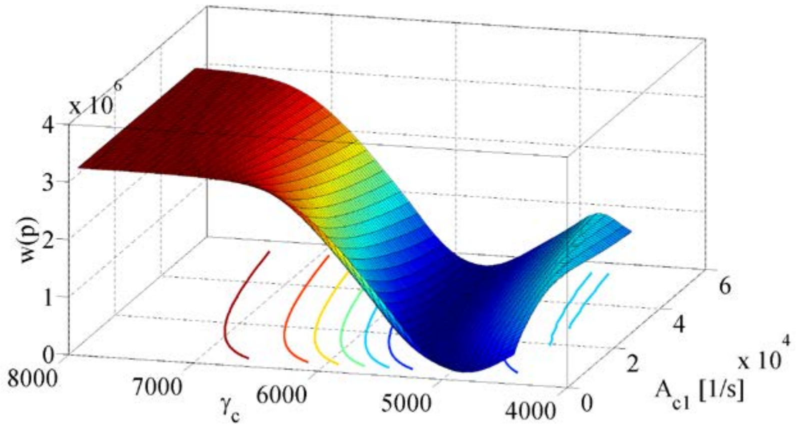

Figure 10. Objective function in equation (19), plotted with respect to A_{c1} and γ_c.